Cleaner Materials 5 (2022) 100104

Contents lists available at ScienceDirect

Cleaner Materials

journal homepage: www.journals.elsevier.com/cleaner-materials

Synthesis of mesoporous akaganeite functionalized maize cob biochar for adsorptive abatement of carbamazepine: Kinetics, isotherms, and thermodynamics

Selly Jemutai-Kimosop [a], Veronica A. Okello [b], Victor O. Shikuku [c,*], Francis Orata [a], Zachary M. Getenga [b]

[a] Department of Chemistry, Masinde Muliro University of Science and Technology, P.O.Box 190, Kakamega, Kenya
[b] Department of Physical Sciences, Machakos University, P.O.Box 136-90100, Machakos, Kenya
[c] Department of Physical Sciences, Kaimosi Friends University College, P.O. Box 385-50309 Kaimosi, Kenya

ARTICLE INFO

Keywords:
Akaganeite
Carbamazepine
Adsorption
Biochar

ABSTRACT

In this work, akaganeite (β-FeO(OH)) impregnated maize cob biochar (Fe-MCB) was prepared by direct hydrolysis, and its adsorptive potential was tested against aqueous solutions of carbamazepine (CBZ), an emerging contaminant. The adsorbent was characterized by standard methods, namely XRD, SEM-EDX, FT-IR, BET surface area analysis, and VSM. Fe-MCB exhibited mesoporous textural structure with paramagnetic behavior at room temperature. The equilibrium data were modeled using the Langmuir, Freundlich, Fowler-Guggenheim and Sips isotherm models. The adsorption data were best described by Fowler-Guggenheim with an estimated maximum adsorption capacity of 81.80 mg g^{-1}. The adsorption rate was described by the pseudo-first-order (PFO) model. The thermodynamic functions, namely enthalpy (ΔH = -6.88 kJ mol^{-1}), negative Gibbs free energy (ΔG) values, entropy (ΔS = 26.33 J mol^{-1}), indicated that the adsorption was exothermic, spontaneous, with the increased disorder at the solid-liquid interphase. The adsorption mechanism is thought to entail dispersive interactions. Modified maize cob biochar is a potentially techno-economic sorbent for CBZ adsorption.

Introduction

Pharmaceutical compounds (PCs) are among the so-called emerging contaminants (ECs) including personal care products, and other industrial products. Following the increasing use of these compounds for disease management, PCs have become common pollutants in drinking (Al-Hamadani et al., 2017). Pharmaceuticals have been found in wastewater, drinking water, and other aquatic systems as a consequence (Jun et al., 2019). Pharmaceutical ingredients have been found in Kenyan aquatic environments, according to recent reports, especially in urban areas (K'oreje et al., 2016; K'oreje et al., 2018; Kairigo et al., 2020; Kimosop et al., 2016; Ngigi et al., 2020; Ngumba et al., 2016). Most recently, Kandie et al. (2020) reported 68 compounds not previously detected in the Kenyan environment including the anti-cancer drugs. Exposure of non-target organisms in the aquatic ecosystem to PCs has been associated with several disorders and biological dysfunctions including the emergence of drug-resistant microbial isolates (Azuma et al., 2019).

Carbamazepine, an anti-seizure drug, has been shown to survive traditional wastewater treatment approaches (Zhang et al., 2008; Kiecak et al., 2019) making the plants as point sources of CBZ loading into recipient waters especially in emerging economies (K'oreje et al., 2020).

Carbamazepine is toxic and a potential carcinogen (Oetken et al., 2005; Kosjek et al., 2009). The different methods for the removal of PCs and emerging contaminants from the water were recently reviewed and the details will not be reiterated here (K'oreje et al., 2020). Adsorption remains the favored method of PCs sequestration from water (Gao et al., 2018).

Among the adsorbents reported for removal of PCs from water are: carbon nanotubes (Deng et al., 2019), biochars (Shikuku and Kimosop, 2020), activated carbons (To et al., 2017), haematites (Rajendran and Sen, 2018), zeolites (Ng'eno et al., 2019), metal-organic frameworks (MOFs) (Jun et al., 2019) and modified diatomaceous earth (Kimosop et al., 2019). Biochars are low-cost sorbents and are particularly significant in sequestration of CBZ from water. Biochars derived from various precursor materials have been evaluated as possible adsorbents

* Corresponding author.
E-mail address: vshikuku@kafuco.ac.ke (V.O. Shikuku).

https://doi.org/10.1016/j.clema.2022.100104
Received 16 March 2022; Received in revised form 6 June 2022; Accepted 12 June 2022
Available online 17 June 2022
2772-3976/© 2022 The Author(s). Published by Elsevier Ltd. This is an open access article under the CC BY-NC-ND license (http://creativecommons.org/licenses/by-nc-nd/4.0/).

for the removal of CBZ from water. These biochar feedstock include peanut shells (Chen et al., 2017), pine white wood (Naghdi et al., 2017), spent coffee grounds (Shin et al., 2020), and pine sawdust (Chu et al., 2019) among other carbonaceous materials (Décima et al., 2021).

The performance of agricultural waste-derived biochars is dependent on the type of waste, sorbent preparation conditions, activation or modification method and the chemistry of the pollutant while the sustainability is dependent on the abundance of biomass (Décima et al., 2021). The structure of akaganeite (β-FeOOH) is made up of iron oxyhydroxide frameworks possessing tunnels partially filled with chloride anions (Holm, 1985). These tunnels imbue akaganeite with properties suitable for encapsulating contaminants from water including heavy metals (Guo and Chen, 2005; Lazaridis et al., 2005), phosphates (Chitrakar et al., 2006), natural organic matter (NOM) (Genz et al., 2008) and as an additive to improve the functionality and adsorption capacity of granular activated carbon (Jang et al., 2008), polyaniline (Shokry et al., 2019), wheat straw biochar (Ji-hui et al., 2014) and other sorbents (Jianhai et al., 2012). Iron oxide has been demonstrated to be a useful additive for ameliorating the adsorption capacity of biochars (Wu et al., 2020; Kim et al., 2019; Yang et al., 2017; Ji-hui et al., 2014). This is because the iron oxides, example magnetite (Fe_3O_4) and maghemite (Fe_2O_3), can form bonds with reactive amide and hydroxide groups present in organic compounds (Shan et al., 2016). However, the applicability depends on the abundance of the biomass, and the preparation requirements for the modified biochar. Though akaganeite has unique properties that can improve the adsorption characteristics of the host material, to date, there is no published work on adsorptive abatement of carbamazepine (CBZ) by akaganeite modified maize cob biochars. Maize being a staple food in Kenya, its abundance and the simple single-step synthesis route makes it a potentially techno-economic adsorbent that can be replicated even in remote regions. This research aimed to evaluate the sorption abatement potential of akaganeite modified maize cob biochar (Fe-MCB) for carbamazepine remotion from water as influenced by several experimental factors. Adsorption kinetics was examined using the pseudo-first (PFO) and pseudo-second-order (PSO) models while isotherm fitting was evaluated using the Langmuir, Freundlich, Fowler-Guggenheim and Sips isotherm models. The model parameters were obtained by non-linear regression and five error functions were used to find the best-fitting model.

Materials and methods

Adsorbent preparation

The maize cob biochar (MCB) was synthesized as described in previous work (Shikuku and Kimosop, 2020). Briefly, the MCB was prepared by slow-pyrolysis at 350 °C at a heating rate of 10 °C min^{-1} and a residence time of 60 min in a furnace. The product was then cleaned with deionized water and oven-dried at 100 °C for 2 h. The clean and dried biochar was then sieved through a 220 μm sieve and modified by impregnation with iron modified by direct hydrolysis following the protocol described by Kimosop et al. (2019). MCB (10 g) was diffused in an iron salt solution containing 10 g of $FeCl_3{\cdot}4H_2O$ in 50 mL of deionized water for 8 h, filtered, then oven-dried at 105 °C for 12 h, and the resultant sorbent (Fe-MCB) sieved through a 220 μm sieve before use. All chemicals were analytical grade purchased from Kobian Scientific (Kenya).

Adsorbent characterization

X-ray fluorescence (XRF) analysis was done for the determination of the elemental composition of the MCB and Fe-MCB. Nitrogen adsorption-desorption at 77 K (Quadrasorb Evo 4, Quantachome, USA) was used to determine the specific surface area of Fe-MCB. Prior to N_2 dosing, about 500–1000 mg of the sample was degassed at 120 °C for 12 h under vacuum. Total surface area and micropore surface area was calculated from experimental isotherms using the Brunauer–Emmett–-Teller (BET) analysis method. The surface functional groups in MCB and Fe-MCB were obtained by a Fourier-transform infrared (FTIR) spectrometer (Nicolet iS-5, USA). The mineral phases present in the biochars were determined using an X-ray Brucker diffractometer (XRD) (D8 Advance) with copper radiation (K_α = 1.5406Å). Surface morphology was inspected using scanning electron microscopy (SEM) (BITRI BSM 6460LV and Zeiss Ultra60). The magnetic behavior of Fe-MCB was determined by a vibrating sample magnetometer (VSM) system (model XL-5).

Adsorption studies

Adsorption studies were carried out in batch mode. A weighed amount (0.1 g) of Fe-MCB was added to a 50 mL solution of carbamazepine (CBZ) (1 mg L^{-1}). The contents were agitated at 120 rpm at 25 °C. The kinetics were evaluated over a period of 6 h with sampling and determination of residual CBZ at time intervals. The effects of initial adsorbate concentration (0.25–1.25 mg L^{-1}), temperature (25–65 °C), and solution pH (2–10) were also examined. High-performance liquid chromatography (HPLC) with ultraviolet (UV) detection (Shimadzu LC 20AT) at 252 nm was used to determine residual carbamazepine (Chen et al., 2016). The CBZ retained in the solid phase at equilibrium (q_e) was obtained using the relation:

$$q_e = \frac{(C_i - C_e)V}{m} \quad (1)$$

The percent adsorbate removal was obtained by the equation:

$$\%R = \frac{(C_i - C_e)}{C_i} \times 100 \quad (2)$$

The initial and equilibrium sorbate concentrations (mg/L) are C_i and C_e, respectively, V is the volume of solution (L), and m is the mass of adsorbent (g). CBZ standard was purchased from Dr. Ehrenstorfer (Germany).

Results and discussion

Elemental composition

The elemental compositions of the pristine biochar (MCB), and the iron-treated biochar (Fe-MCB) indicated an appreciable increase in iron, from 53.94 to 74.88 % in the sorbent (Table 1). The variations in chemical composition of other elements are possibly due to ion exchange or into solution during hydrolysis.

Surface morphology

The surface morphology of MCB and Fe-MCB as depicted in the SEM micrographs portray visible differences in surface structural features of the two materials. The pristine MCB (Fig. 1(a)) seems to possess a highly porous sponge-like structure with relatively large interconnected pores, unlike the Fe-MCB that portrayed a matrix of discontinuities and akaganeite particles spread on the surface (Fig. 1(b)).

Table 1
Elemental percent (%) composition of the biochars by XRF.

	Fe	K	Cl	Zn
MCB	53.94	26.24	19.43	0.40
Fe-MCB	74.88	3.13	22.00	n.d

*n.d-not detected.

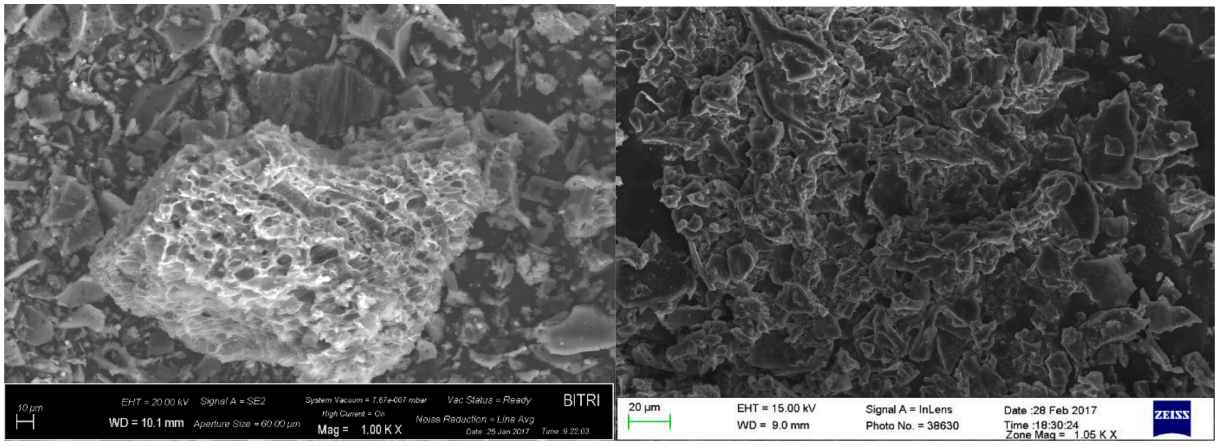

Fig. 1. SEM micrograph of (a) MCB (b) Fe-MCB.

XRD analysis

The diffractogram for maize cob biochar (MCB) (Fig. 2) revealed peaks characteristic of quartz (SiO_2). The diffraction peaks at 2θ values of 26.40°, 34.91°, 38.99°, 55.53°, 60.98° and 77.41° in the MCB diffractogram are typical of sylvite (Fig. 2). After chemical treatment, the Fe-MCB diffraction peaks at 28.22°(310), 34.71°(400), 40.40°(301), 49.94°(530), 55.56°(521), 58.51°(002), 66.23°(541) and 73.57° (Fig. 3) are characteristic of tetragonal Akaganeite (β-FeO(OH)) structure (Joint Committee on Powder Diffraction Standards (JCPDS) No. 34–1266). Other iron-oxide phases possibly present include magnetite and maghemite though their identification by XRD method is complex since they both have the same cubic structure, and their lattice parameters are almost identical (Ebrahim et al., 2016).

FTIR analysis

The FT-IR spectra for MCB and Fe-MCB are presented in Fig. 4. The structural –OH stretching vibration and outer –OH groups from surface adsorbed water was ascribed to the broad absorption band at 3600–3700 cm^{-1} (Namduri and Nasrazadani, 2008). These bands (3600–3300 cm^{-1}) in the Fe-MCB were sharp and pronounced relative to MCB. This suggests an increase in hydroxyl groups which are potential binding sites for organic adsorbates. The absorption bands at 1597 cm^{-1} are assigned to carbonyl (C═O) stretch, while those at 1339 and 1350 cm^{-1} are attributed to metal oxide. The bands at 633 and 667 cm^{-1} were ascribed to Fe-O vibration signals of iron oxide (Shikuku et al., 2018b). The band around 764 cm^{-1} is attributed to C—H vibrations. The relative change in band broadness and increase in intensity of absorption peaks in Fe-MCB compared to MCB such as C═O and Fe-O stretching bands indicates the interaction between the biochar and akaganeite particles (Ebrahim et al., 2016).

Textural analysis

The BET surface area of Fe-MCB was 2.58 $m^2\ g^{-1}$. The calculated total pore volume was found to be 0.0306 $cm^3\ g^{-1}$ with an average pore size of 30.15 nm corresponding to mesoporous materials. Since the equivalent Stokes radius of carbamazepine calculated by the Wilke-Chang and the Stokes-Einstein equations is 0.37 nm (Nghiem et al.,

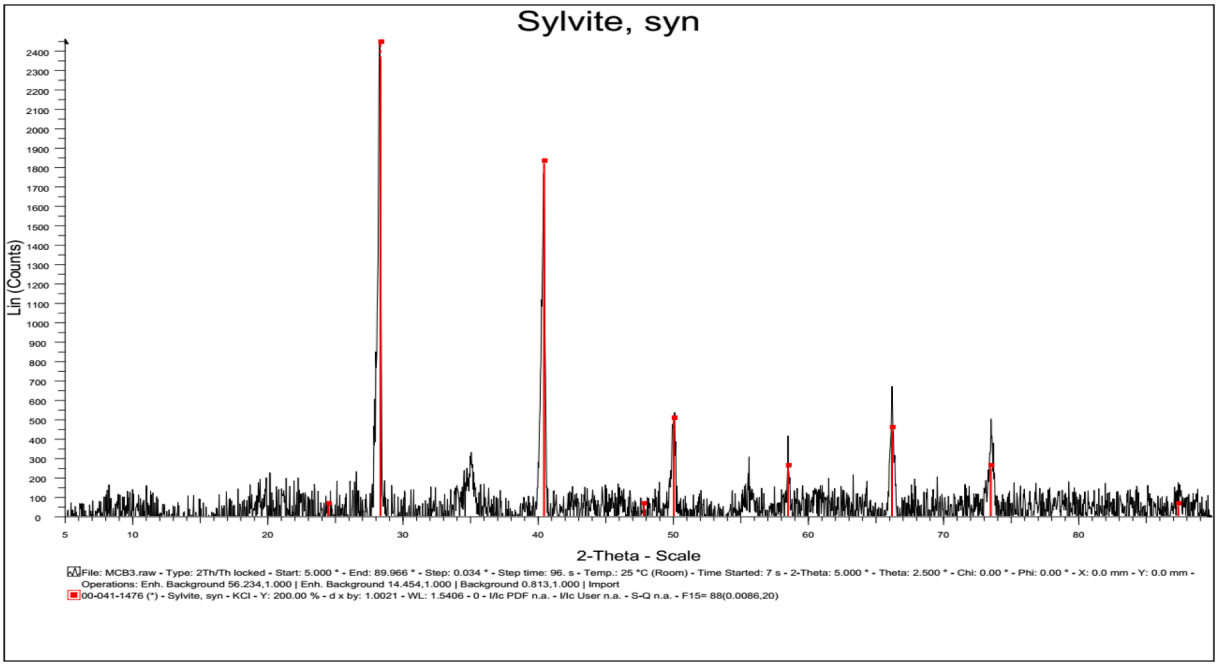

Fig. 2. The XRD pattern for maize cob biochar (MCB).

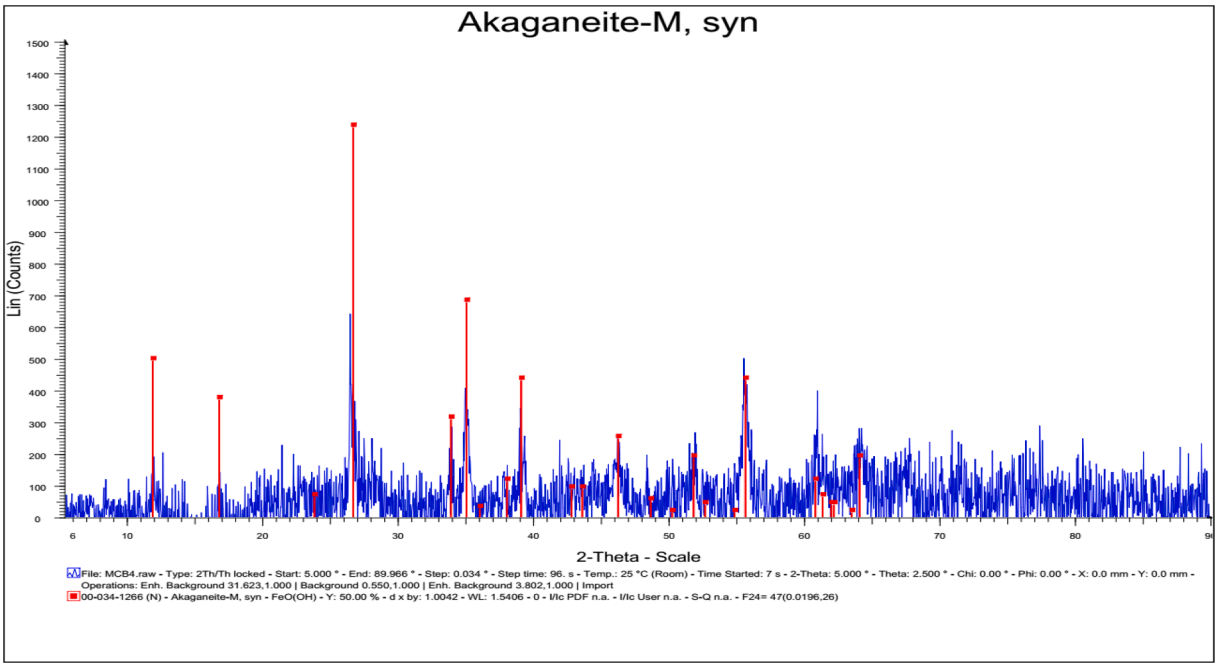

Fig. 3. The XRD pattern for akaganeite modified maize cob biochar (Fe-MCB).

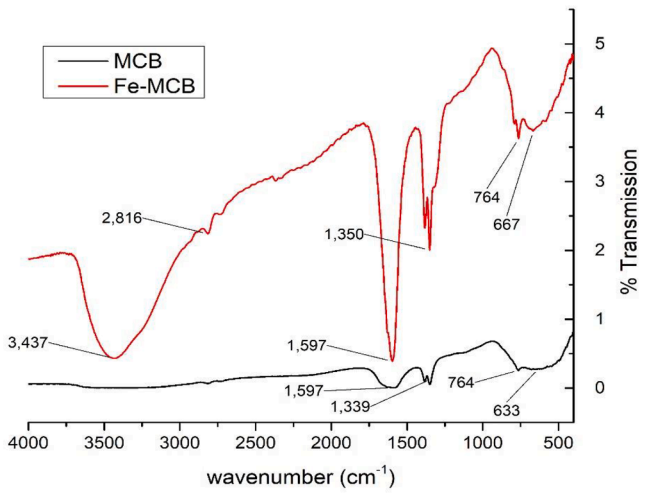

Fig. 4. FTIR spectra of MCB and Fe-MCB.

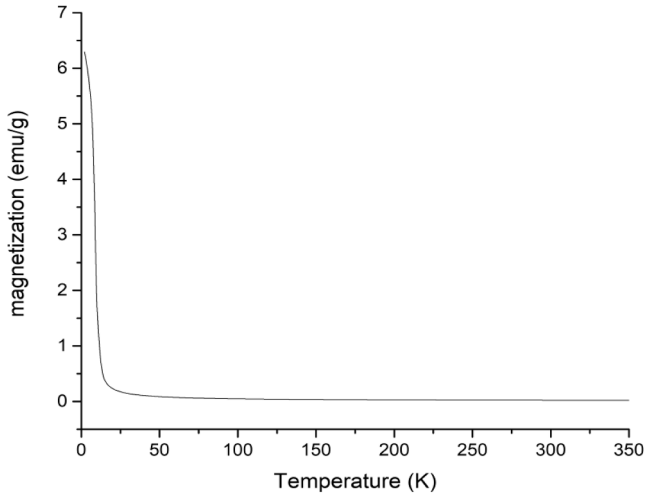

Fig. 5. Magnetic hysteresis loop for Fe-MCB adsorbent.

2005), much smaller than the Fe-MCB average pore size, convective transport of the carbamazepine through the pores of this adsorbent is considered certain.

Magnetic measurement

Magnetic responsiveness can be utilized in recovering an exhausted adsorbent from the aqueous solution (Zhang et al., 2013). The magnetic properties of Fe-MCB adsorbent, as depicted in the hysteresis curve (Fig. 5), exhibited ferromagnetic properties and the magnetization decreased with an increase in temperature and becomes paramagnetic beyond 25 K due to the disorderliness of the magnetic moments. At room temperature (293–298 K), the material possessed extremely weak magnetization to be recoverable by an external magnetic field.

Adsorption kinetics

The amount of carbamazepine (CBZ) sequestered with time by Fe-MCB attained a maximum in about 120 min (Fig. 6) followed by equilibrium with no appreciable change in the amount in the solid phase. The equilibration is a consequence of the saturation of the binding sites.

The kinetic data was further tested using the pseudo-first-order (PFO) (Ho and McKay, 1998) and pseudo-second-order (PSO) (Ho, 2006) rate equations using nonlinear regression. The applicability of the model to describe the reaction kinetics was decided based on four error functions: Hybrid fractional error function (HYBRID), Marquart's percentage standard deviation (MPSD), Sum of squares error (SSE), and Average relative error (ARE) (Table 2) and the closeness between experimental (q_{exp}) and model-predicted (q_{cal}) equilibrium adsorption capacities. The calculated kinetic models' parameters are presented in Table 3.

$$Pseudo-first-order(PFO)\ \ mod\ el: q_t = q_e\left(1-\ell^{-k_1 t}\right)$$

$$Pseudo-second-order(PSO)\ \ mod\ el: q_t = \frac{q_e^2 k_2 t}{1+k_2 q_e t}$$

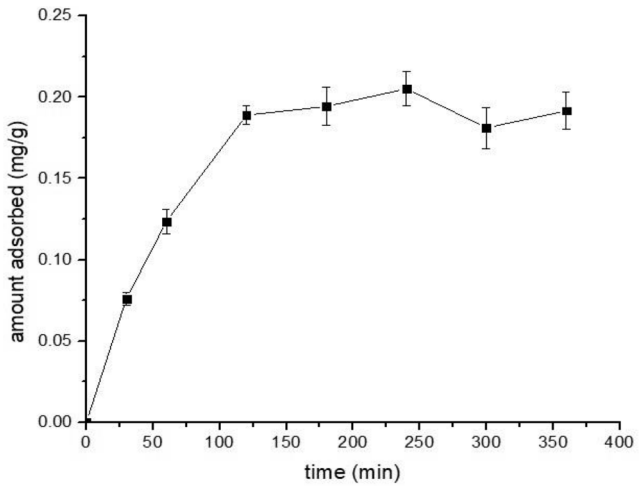

Fig. 6. Variation of adsorption of CBZ by Fe-MCB with time (C_o = 1 mg/L, dose = 0.1 g/50 mL).

Table 2
Error functions used in the study.

Error function	Equation	Definition of parameters
HYBRID	$\frac{100}{n-p}\sum_{i=1}^{n}\frac{\left(q_{e(exp)}-q_{e(cal)}\right)^2}{q_{e(exp)}}$	$q_{e(exp)}$: experimental observations $q_{e(cal)}$: calculated values n: the number of observations in the experimental data; p: the number of parameters in the isotherm model.
MPSD	$100\left(\sqrt{\frac{1}{n-p}\sum_{i=1}^{n}\frac{\left(q_{e(exp)}-q_{e(cal)}\right)^2}{q_{e(exp)}}}\right)$	
EABS	$\sum_{i=1}^{n}\lvert\left(q_{e(cal)}-q_{e(exp)}\right)\rvert$	
Chi-square (χ^2)	$\sum_{i=1}^{n}\frac{\left(q_{e(cal)}-q_{e(exp)}\right)^2}{q_{e(exp)}}$	
Average relative error (ARE)	$\frac{100}{n}\sum_{i=1}^{n}\frac{\left(q_{e(exp)}-q_{e(cal)}\right)}{q_{e(exp)}}$	

Table 3
Calculated kinetics parameters.

Kinetic model	PFO	PSO
Parameters	$q_{e(cal)}$ mg g^{-1} = 0.165 K_1 min^{-1} = 3.00 $q_{e(exp)}$ mg g^{-1} = 0.170	$q_{e(cal)}$ mg g^{-1} = 0.106 K_2 g $mg^{-1}min^{-1}$ = 0.006 $q_{e(exp)}$ mg g^{-1} = 0.170
HYBRID	1.960	2.88
MPSD	14.00	16.99
ARE	24.32	32.45

Based on the error functions and the degree of variance between the experimental (q_{exp}) and the model-predicted (q_{cal}) equilibrium adsorption capacities, the pseudo-first-order (PFO) model better predicted the adsorption kinetics relative to the pseudo-second-order (PSO) equation. Fig. 7 represents the comparative fitting of the experimental data to the kinetic models. The PFO model postulates physisorption governed rate-controlling step.

Isotherm modeling

The equilibrium data were fitted to four adsorption isotherms (Langmuir, Freundlich, Fowler-Guggenheim, and Sips isotherms) to predict the adsorption mechanisms. The isotherm parameters were calculated by the nonlinear regression method by minimization of regression sum of squares (RSS) function defined by equation (5).

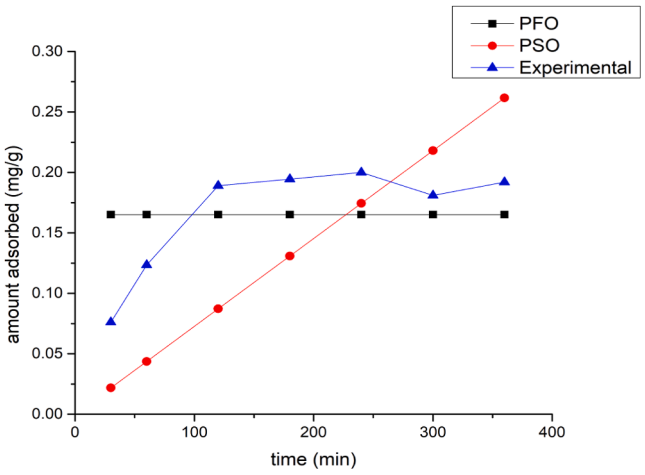

Fig. 7. Comparison of predictive ability of PFO and PSO models to the experimental data (C_o = 1 mg/L, dose = 0.1 g/50 mL).

$$RSS = \sum_{1}^{N}\left(q_{e,experimental} - q_{e,predicted}\right)^2 \quad (5)$$

The mathematical error functions presented in Table 2 were used to find the best-fitting model (Shikuku et al., 2018a; Zheng et al., 2019).

Langmuir isotherm

The Langmuir isotherm (Langmuir, 1916) proposes monolayer adsorption of adsorbate molecules onto a morphologically homogeneous adsorbent surface with a fixed number of energetically equal adsorption sites with no lateral interaction. The Langmuir equation is given as:

$$q_e = \frac{Q_0 K_L C_e}{1 + K_L C_e} \quad (6)$$

Where q_e represents the amount of adsorbate adsorbed per unit mass of the sorbent at equilibrium (mg g^{-1}), C_e is the residual adsorbate concentration in the solution at equilibrium (mg L^{-1}), Q_0 denotes the maximum adsorption capacity (mg g^{-1}) and K_L is the Langmuir constant (L mg^{-1}). Relative to the other isotherms, high values of the calculated error functions (Table 4) denote that the assumptions of the Langmuir model cannot account for the adsorption mechanism of CBZ onto the modified sorbent, Fe-MCB. The inability of the Langmuir model to predict the adsorption of CBZ has been reported earlier, for iron-modified diatomaceous earth (Kimosop et al., 2019). The relative fitting of the isotherms to experimental data is shown in Fig. 8.

Freundlich isotherm

The Freundlich isotherm (Freundlich, 1906) assumes no lateral interactions between the adsorbed moieties and assumes a multilayer adsorption process onto a heterogeneous adsorbent surface. The Freundlich isotherm is given as:

Table 4
Adsorption isotherm parameters.

Isotherm	Langmuir	Freundlich	Fowler-Guggenheim	Sips
Parameters	Q_0 = 0.019 K_L = 0.345	1/n = 1.903 K_F = 0.581	W = -3514.5 K_{FG} = 0.387	a_s = 0.007 q_{MS} = 81.802 B_s = 1.907
EABS	2.248	1.208	0.395	1.206
ARE	44.962	24.159	7.905	24.133
HYBRID	5.543	1.766	1.099	2.645
χ^2	0.097	0.044	0.035	0.044
MPSD	23.543	13.289	10.488	16.264

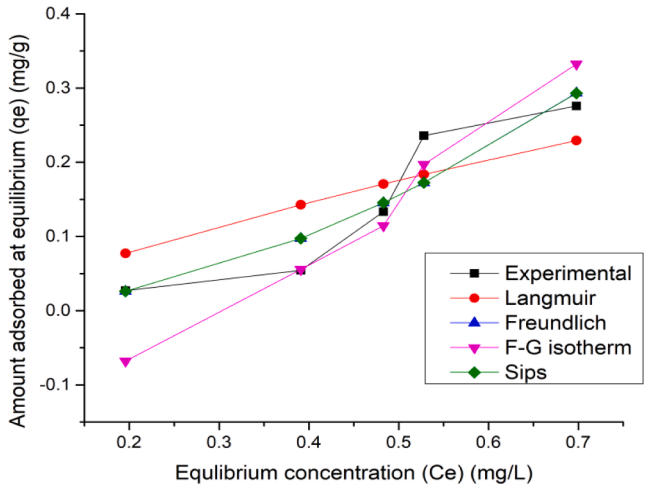

Fig. 8. Adsorption isotherms for CBZ uptake by Fe-MCB (C_o = 0.25–1.25 mg/L, dose = 0.1 g/50 mL).

$$q_e = K_F C_e^{1/n} \tag{7}$$

Where K_F is the Freundlich constant (L/mg) and n is a dimensionless constant.

The data were also fitted to the Freundlich model and the constants presented in Table 4. The Freundlich model predicted the experimental data better than the Langmuir isotherm but also fitted poorly relative to the other isotherms tested. Furthermore, the magnitude of n (0.525) would suggest a poor adsorption process (Treybal, 1981) while the 1/n suggests weaker adsorbate-adsorbent interactions corresponding to suggesting a physisorption mechanism (To et al., 2017).

The Fowler-Guggenheim isotherm

The Fowler-Guggenheim (F-G) model (Fowler and Guggenheim, 1939) considers the adsorbate species' lateral interactions in the solid phase. The Fowler-Guggenheim equation is expressed as:

$$C_e = \frac{\theta_{FG}}{K_{FG}(1-\theta_{FG})}\exp\left(\frac{2\theta_{FG}W}{RT}\right) \tag{8}$$

where K_{FG} is the Fowler–Guggenheim equilibrium constant (L mg^{-1}), θ the fractional coverage, R the gas constant (kJ mol^{-1} K^{-1}), T the temperature (K), and W is an index of the interaction energy between adsorbed molecules (kJ mol^{-1}).

In describing the adsorbate-adsorbate interactions for adsorbed molecules, when W is positive, the interactions are attractive. Negative W, on the other hand, signifies repulsive interactions. When no adsorbate-adsorbate interaction exists between the adsorbed molecules, W = 0. Based on the error functions (Table 4), the adsorption of CBZ onto Fe-MCB was best described by the Fowler-Guggenheim isotherm model. The negative W value indicates repulsive interactions between the adsorbed CBZ molecules (Shikuku and Mishra, 2021).

Sips isotherm

The Sips isotherm (Sips, 1948) combines the Freundlich and Langmuir isotherms and is used in heterogeneous adsorption where the adsorbed molecule has multiple adsorption sites. The model, however, does not account for adsorbate-adsorbate synergy. The Sips isotherm is expressed as:

$$q_e = \frac{q_{ms}a_s C_e^{B_s}}{1 + a_s C_e^{B_s}} \tag{9}$$

Where q_{ms}, a_s and B_s are the isotherm constants. The constant B_s is the heterogeneity index whose magnitude increases with heterogeneity. Furthermore, as stated in the Langmuir equation, values closest to unity imply a homogenous adsorbent surface. The experimental sorption data were acceptably describable by the Sips model as depicted by the error function values (Table 4). The B_s parameter (1.924) denotes adsorption on a heterogeneous adsorbent surface. The predicted maximum adsorption capacity was 81.80 mg g^{-1}. Overall, the equilibrium data were described by the isotherms in the order Fowler-Guggenheim > Sips > Freundlich > Langmuir. The performance of Fe-MCB was compared to modified biochars from different feedstock and the details are summarized in Table 5. It is shown that Fe-MCB has appreciably high adsorption capacity under comparable experimental conditions.

Effect of pH

The solution pH affects both the surface chemistry and the dissociation of organic compounds in solution that have a direct effect on the adsorption efficiency and mechanism. The effect of pH on (CBZ) uptake by Fe-MCB was evaluated and the results are presented in Fig. 9.

CBZ removal efficiency was strongly dependent on the solution pH with the least percent removal noted at pH 6. Insight on the possible adsorption mechanisms was elucidated by a comparison of the dissociation constant of CBZ and sorbent's pH of point of zero charge.

The hydroxyl groups with a reported pK_a 9.5–13 (Volesky, 2007) would be protonated at pH below 13, as in the experimental conditions, and so the surface charge of the sorbent (pH_{pzc}, 5.6) was positively charged. CBZ is reported to have the following pK_a values; pK_{a1} at 2.30 (ketone group) and pK_{a2} 13.90 (amine group) (Punyapalakul and Sitthisorn, 2010). This implies that between pH 2–10, CBZ molecules were present as neutral species (CBZ^0). This excludes electrostatic forces as the driving adsorption mechanism. Additionally, the net positive surface charge of Fe-MCB (C-$FeOOH_2^+$) (pH_{pzc} = 5.6) implies reduced availability of oxygen functional groups to form Lewis acid-base complexes or hydrogen bonding. These adsorption mechanisms are therefore minimal. CBZ being a hydrophobic molecule, dispersive interactions which are low-energy interactions are proposed as the predominant adsorption mechanism. Nevertheless, specific interactions with the functional groups in the pores of the sorbent with the urea moiety of CBZ cannot be ruled out (Nielsen et al., 2014) or interactions between the positively charged $FeOOH_2^+$, $[C\text{-}Fe(OH_2)_5]^{3+}$, $[C\text{-}Fe(OH_2)_4(OH)]^{2+}$ on the Fe-MCB surface and the π-electron system of CBZ. The decreased adsorption at pH 6 could be attributed to weak electrostatic interactions (Liang et al., 2020).

Adsorption thermodynamics

Adsorption processes are temperature dependent reactions. In this work, the dependence of the uptake of CBZ by Fe-MCB on temperature was examined in the range (25–65 °C). The thermodynamic parameters, ΔG, ΔH and ΔS, were computed using the following equations:

$$\Delta G = -RT\ln K_c \tag{10}$$

$$K_d = \frac{q_e}{C_e} \tag{11}$$

$$K_c = 1000K_d \tag{12}$$

$$\ln K_c = \frac{\Delta S}{R} - \frac{\Delta H}{R}\frac{1}{T} \tag{13}$$

Where K_c is the equilibrium constant (dimensionless), C_e is the amount of CBZ in solution (mg L^{-1}) and q_e is the amount of CBZ in the adsorbent (mg g^{-1}), at equilibrium. R and T are as previously defined.

The decrease in removal efficiency (Table 6) as temperature rises denotes that the adsorption reaction is an exothermic process and is consistent with the negative Δ H reported. The negative Δ G values correspond to a thermodynamically spontaneous. The very low

Table 5
Comparison of CBZ adsorption by various modified biochars.

Adsorbent	Feedstock	Modification	Initial concentration (mg/L)	Adsorption capacity (mg/g)	Postulated Mechanism	Reference
HBC300	Peanut shells	HCl 1 M washed	1.0–50 mg/L	14.81	Hydrophobic Interaction π- π bonding interactions	Chen et al. (2017)
FBC300	Peanut shells	HCl/HF 1:1 1 M washed	1.0–50 mg/L	6.84	Hydrophobic interaction π- π bonding interactions	Chen et al. (2017)
HBC500	Peanut shells	HCl 1 M washed	1.0–50 mg/L	4.96	Hydrophobic interaction π- π bonding interactions	Chen et al. (2017)
FBC500	Peanut shells	HCl/HF 1:1 1 M washed	1.0–50 mg/L	3.95	Hydrophobic Interaction π- π bonding interactions	Chen et al. (2017)
SGC biochar	Spent coffee grounds	Alkaline modification	1.0–10 mg/L	91.74	Pore-filling effects, Electrostatic interaction, Hydrophobic interactions	Shin et al. (2020)
CBC	Cauliflower roots	$CuO/Cu_2O/Cu$	n.a	19.4	Hydrogen bonding, π- π bonding interactions	Liang et al. (2020)
Biochar/ Fe_3O_4	Coconut/pinenut/ walnut shells	Fe_3O_4	5–60 mg/L	62.7	n.a	Shan et al. (2016)
BL300	Pine sawdust	Bleaching treatment	0.1–5.0 mg/L	0.04	n.a	Chu et al. (2019)
BL700	Pine sawdust	Bleaching treatment	0.1–5.0 mg/L	0.32	n.a	Chu et al. (2019)
Fe-MCB	Maize cobs	akaganeite	0.25–1.25 mg/L	81.80	Dispersive interactions	This study

n.a- not applicable/not reported in the study.

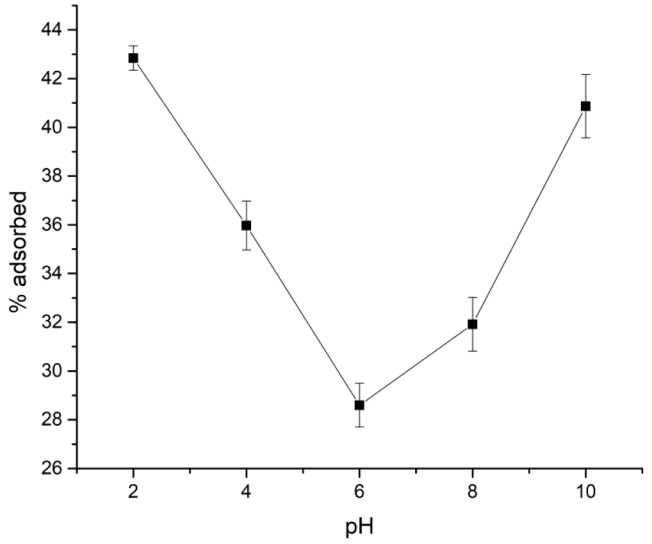

Fig. 9. Effect of solution pH on CBZ adsorption onto Fe-MCB.

Table 6
Calculated thermodynamic parameters.

Compound	Temp. (K)	% removal	ΔG (kJ mol^{-1})	ΔH (kJ mol^{-1})	ΔS (kJ mol^{-1})
CBZ	298	43.00	−14.70	−6.88	26.33
	308	41.08	−14.99		
	318	39.56	−15.31		
	328	37.55	−15.55		
	338	34.98	−15.72		

magnitude of ΔH (6.880 kJ mol^{-1}), attests that the physisorption accounts for the adsorption mechanism of CBZ onto Fe-MCB with no exchange of electrons involved (Shikuku et al., 2015; Tome et al., 2021). This is consistent with the proposed dispersive interactions adsorption mechanism and predictions of the PFO model.

Conclusion

In this work, maize cob biomass, an abundant agricultural waste, was carbonized and the resulting biochar (MCB) was chemically modified with akaganeite (β-FeO(OH)) by hydrolysis to induce increased surface functionality. The resulting sorbent (Fe-MCB) was applied for the adsorptive remotion of carbamazepine (CBZ) from simulated wastewater. The sorption data were best described by the Fowler-Guggenheim and Sips isotherm models with a maximum adsorption capacity of 81.8 mg/g. The pseudo-first-order (PFO) law predicted the adsorption rate, achieving equilibrium in 120 min. The adsorption reaction was thermodynamically favorable, spontaneous (ΔG = -14.70 kJ/mol at 298 K), exothermic (ΔH = -6.88 kJ/mol), and physical. Although other functional group-specific interactions are possible, dispersive interactions are thought to be the most probable adsorption mechanism. The adsorption capacity of Fe-MCB was comparable and superior to those reported in literature for CBZ removal from water.

Declaration of Competing Interest

The authors declare that they have no known competing financial interests or personal relationships that could have appeared to influence the work reported in this paper.

Funding

The International Foundation for Science (IFS) funded this research with grant number W/5587-1.

References

Al-Hamadani, Y.A.J., Park, C.M., Assi, L.N., Chu, K.H., Hoque, S., Jang, M., Yoon, Y., Ziehl, P., 2017. Sonocatalytic removal of ibuprofen and sulfamethoxazole in the presence of different fly ash sources. Ultrason. Sonochem. 39, 354–362.

Azuma, T., Kana, O., Shiori, M., Mao, I., Kanae, H., Ayami, Y., Yoshiki, M., Tetsuya, H., 2019. Environmental fate of pharmaceutical compounds and antimicrobial-resistant bacteria in hospital effluents, and contributions to pollutant loads in the surface waters in Japan. Sci. Total Environ. 657, 476–484. https://doi.org/10.1016/j.scitotenv.2018.11.433.

Chen, J., Zhang, D., Zhang, H., Ghosh, S., Pan, B., 2017. Fast and slow adsorption of carbamazepine on biochar as affected by carbon structure and mineral composition. Sci. Total Environ. 579, 598–605.

Chitrakar, R., Tezuka, S., Sonoda, A., Sakane, K., Ooi, K., Hirotsu, T., 2006. Phosphate adsorption on synthetic goethite and akaganeite. J. Colloid Interface Sci. 298, 602–608.

Chu, G., Zhao, J., Liu, Y., Lang, D., Wu, M., Pan, B., Steinberg, C.E.W., 2019. The relative importance of different carbon structures in biochars to carbamazepine and bisphenol A sorption. J. Hazard. Mater. 373, 106–114.

Décima, M.A., Marzeddu, S., Barchiesi, M., Di Marcantonio, C., Chiavola, A., Boni, M.R., 2021. A Review on the Removal of Carbamazepine from Aqueous Solution by Using Activated Carbon and Biochar. Sustainability. 13, 11760.

Deng, Y., Ok, Y., Mohan, D., Pittman, C., Dou, X., 2019. Carbamazepine removal from water by carbon dot-modified carbon nanotubes. Environ. Res. 169, 434–444.
Ebrahim, S., Shokry, A., Ibrahim, H., Soliman, M., 2016. Polyaniline/akaganéite nanocomposite for detoxification of noxious Cr(VI) from aquatic environment. J. Polym. Res. 23, 79–85.
Fowler, R.H., Guggenheim, E.A., 1939. Statistical Thermodynamics. Cambridge University Press, London, pp. 431–450.
Freundlich, H.M.F., 1906. U¨ber die adsorption in lo¨sungen. Z. Phys. Chem. 57, 385–470.
Gao, Y., Liu, K., Kang, R., Xia, J., Yu, G., Deng, S., 2018. A comparative study of rigid and flexible MOFs for the adsorption of pharmaceuticals: kinetics, isotherms and mechanisms. J. Hazard. Mater. 359, 248–257.
Genz, A., Baumgarten, B., Goernitz, M., Jekel, M., 2008. NOM removal by adsorption onto granular ferric hydroxide: Equilibrium, kinetics, filter and regeneration studies. Water Res. 42, 238–248.
Guo, X., Chen, F., 2005. Removal of arsenic by bead cellulose loaded with iron oxyhydroxide from groundwater. Environ. Sci. Technol. 39, 6808–6818.
Ho, Y.S., 2006. Review of second-order models for adsorption systems. J. Hazard. Mater. 136, 681–689.
Ho, Y.S., McKay, G., 1998. Sorption of dye from aqueous solution by peat. Chem. Eng. J. 70, 115–124.
Holm, N.G., 1985. New evidence for a tubular structure of β-iron(III) oxide hydroxide-akaganéite. Origins Life Evol. Biosphere 15, 131–139.
Jang, M., Chen, W., Cannon, F.S., 2008. Preloading hydrous ferric oxide into granular activated carbon for arsenic removal. Environ. Sci. Technol. 42, 3369–3374.
Jianhai, Z., Wei, L., Qigang, C., Wenpu, L., Yanping, L., 2012. Adsorptive characteristics of akaganeite and its environmental applications: a review. Environ. Technol. Rev. 1 (1), 114–126.
Ji-hui, L., Guo-hua, L., Wen-bo, B., Qi, L., Yuan-cheng, Z., Ji-qing, S., 2014. Modification and use of biochar from wheat straw (*Triticum aestivum L.*) for nitrate and phosphate removal from water. Desalin. Water Treat. 57, 1–13.
Jun, B.M., Kim, S., Heo, J., Her, N., Jang, M., Park, C.M., Yoon, Y., 2019. Enhanced sonocatalytic degradation of carbamazepine and salicylic acid using a metal organic framework. Ultrason. Sonochem. 56, 174–182.
K'oreje, K.O., Vergeynst, L., Ombaka, D., De Wispelaere, P., Okoth, M., Van Langenhove, H., Demeestere, K., 2016. Occurrence patterns of pharmaceutical residues in wastewater, surface water and groundwater of Nairobi and Kisumu city, Kenya. Chemosphere 149, 238–244. https://doi.org/10.1016/j.chemosphere.2016.01.095.
K'oreje, K.O., Kandie, F.J., Vergeynst, L., Abira, M.A., Van Langenhove, H., Okoth, M., Demeestere, K., 2018. Occurrence, fate and removal of pharmaceuticals, personal care products and pesticides in wastewater stabilization ponds and receiving rivers in the Nzoia Basin. Kenya. Sci Total Environ. 637–638, 336–348.
K'oreje, K.O., Okoth, M., Van Langenhove, H., Demeestere, K., 2020. Occurrence and treatment of contaminants of emerging concern in the African aquatic environment: Literature review and a look ahead. J Environ Manage 254, 109752.
Kairigo, P., Ngumba, E., Sundberg, L.R., Gachanja, A., Tuhkanen, T., 2020. Occurrence of antibiotics and risk of antibiotic resistance evolution in selected Kenyan wastewaters, surface waters and sediments. Sci Total Environ 720, 137580.
Kandie, F., Krauss, M., Beckers, L., Massei, R., Fillinger, U., Becker, J., Liess, M., Torto, B., Brack, W., 2020. Occurrence and risk assessment of organic micropollutants in freshwater systems within the Lake Victoria South Basin, Kenya. Science of The Total Environment, 136748–. doi:10.1016/j.scitotenv.2020.136748.
Kiecak, A., Lara, S., Mercè, B., Elsner, M., Mas-Pla, J., Salle, C., Stumpp, C., 2019. Sorption properties and behaviour at laboratory scale of selected pharmaceuticals using batch experiments. J. Contamin. Hydrol. 225, 103500.
Kim, J., Song, J., Lee, S., Jung, J., 2019. Application of iron modified biochar for arsenite removal and toxicity reduction. J. Industr. Eng. Chem. 80, 17–22. https://doi.org/10.1016/j.jiec.2019.07.026.
Kimosop, S.J., Getenga, Z.M., Orata, F., Okello, V.A., Cheruiyot, J.K., 2016. Residue levels and discharge loads of antibiotics in wastewater treatment plants (WWTPs), hospital lagoons, and rivers within Lake Victoria Basin, Kenya. Environ Monit Assess 188, 1–9.
Kimosop, S.J., Orata, F., Shikuku, V.O., Okello, V.A., Getenga, Z.M., 2019. Insights on adsorption of carbamazepine onto iron oxide modified diatomaceous earth: Kinetics, isotherms, thermodynamics, and mechanisms. Environ. Res. 108898– https://doi.org/10.1016/j.envres.2019.108898.
Kosjek, T., Andersen, H.R., Kompare, B., Ledin, A., 2009. Fate of carbamazepine during water treatment. Environ. Sci. Technol. 43, 6256–6261.
Langmuir, I., 1916. The constitution and fundamental properties of solids and liquids. J. Am. Chem. Soc. 38, 2221–2295.
Lazaridis, N.K., Bakoyannakis, D.N., Deliyanni, E.A., 2005. Chromium(VI) sorptive removal from aqueous solutions by nanocrystalline akaganeite. Chemosphere 58, 65–73.
Liang, G., Hu, Z., Wang, Z., et al., 2020. Effective removal of carbamazepine and diclofenac by CuO/Cu_2O/Cu-biochar composite with different adsorption mechanisms. Environ Sci Pollut Res 27, 45435–45446. https://doi.org/10.1007/s11356-020-10284-3.
Naghdi, M., Taheran, M., Pulicharla, R., Rouissi, T., Brar, S.K., Verma, M., Surampalli, R. Y., 2017. Pine-wood derived nanobiochar for removal of carbamazepine from aqueous media: Adsorption behavior and influential parameters. Arab. J. Chem. 12, 5292–5301.
Namduri, H., Nasrazadani, S., 2008. Quantitative analysis of iron oxides using Fourier transform infrared spectrophotometry. Corr. Sci. 50, 2493–2497.
Ng'eno, E., Shikuku, V.O., Orata, F., Lilechi, D.B., Kimosop, S., 2019. Caffeine and Ciprofloxacin Adsorption from water onto clinoptilolite: Linear isotherms, kinetics, thermodynamics and mechanistic studies. S. Afr. J. Chem. 72, 136–142.
Nghiem, D.L., Schäfer, A.I., Elimelech, M., 2005. Pharmaceutical retention mechanisms by nanofiltration membranes. Environ. Sci. Technol. 39 (19), 7698–7705.
Ngigi, A.N., Magu, M.M., Muendo, B.M., 2020. Occurrence of antibiotics residues in hospital wastewater, wastewater treatment plant, and in surface water in Nairobi County. Kenya. Environ Monit Assess 192, 18. https://doi.org/10.1007/s10661-019-7952-8.
Ngumba, E., Gachanja, A., Tuhkanen, T., 2016. Occurrence of selected antibiotics and antiretroviral drugs in Nairobi river basin. Sci. Total Environ. 539, 206–213.
Nielsen, L., Biggs, M.J., Skinner, W., Bandosz, T.J., 2014. The effects of activated carbon surface features on the reactive adsorption of carbamazepine and sulfamethoxazole. Carbon 80, 419–432. https://doi.org/10.1016/j.carbon.2014.08.081.
Oetken, M., Nentwig, G., Loffler, D., Ternes, T., Oehlmann, J., 2005. Effects of pharmaceuticals on aquatic invertebrates. Part I. The antiepileptic drug carbamazepine. Arch Environ Contam. Toxicol. 49, 353–361.
Punyapalakul, P., Sitthisorn, T., 2010. Removal of Ciprofloxazin and Carbamazepine by Adsorption on Functionalized Mesoporous Silicates. World Academy Sci. Eng. Technol. 69, 546–550.
Rajendran, K., Sen, S., 2018. Adsorptive removal of carbamazepine using biosynthesized hematite nanoparticles. Environ. Nanotechnol. Monit. Manag. 122–127.
Shan, D., Deng, S., Zhao, T., Wang, B., Wang, Y., Huang, J., Yu, G., Winglee, J., Wiesner, R., 2016. Preparation of ultrafine magnetic biochar and activated carbon for pharmaceutical adsorption and subsequent degradation by ball milling. J. Hazard. Mater. 305, 156–163.
Shikuku, V.O., Kimosop, S., 2020. Efficient Removal of Sulfamethoxazole onto Sugarcane Bagasse-derived Biochar: Two and Three-parameter Isotherms, Kinetics and Thermodynamics. S. Afr. J. Chem. 73, 111–119.
Shikuku, V.O., Mishra, T., 2021. Adsorption isotherm modeling for methylene blue removal onto magnetic kaolinite clay: A comparison of two-parameter isotherms. Appl. Water Sci. 11, 103. https://doi.org/10.1007/s13201-021-01440-2.
Shikuku, V.O., Donato, F.F., Kowenje, C.O., Zanella, R., Prestes, O.D., 2015. A comparison of adsorption equilibrium, kinetics and thermodynamics of aqueous phase clomazone between Faujasite X and a Natural zeolite from Kenya. S. Afr. J. Chem. 68, 245–252.
Shikuku, V.O., Kowenje, C.O., Kengara, F., 2018a. Errors in Parameters Estimation using Linearized Adsorption Isotherms: Sulfadimethoxine Adsorption onto Kaolinite Clay. Chem. Sci. Int. J. 23 (4), 1–6.
Shikuku, V.O., Zanella, R., Kowenje, C.O., Donato, F.F., Bandeira, N., Prestes, O.D., 2018b. Single and Binary Adsorption of sulphonamide antibiotics onto iron-modified clay: Linear and nonlinear Isotherms, Kinetics, thermodynamics and mechanistic studies. Appl. Water Sci. 8, 175. https://doi.org/10.1007/s13201-018-0825-4.
Shin, J., Lee, Y.G., Lee, S.H., Kim, S., Ochir, D., Park, Y., Kim, J., Chon, K., 2020. Single and competitive adsorptions of micropollutants using pristine and alkali-modified biochars from spent coffee grounds. J. Hazard. Mater. 400, 123102.
Shokry, A., El Tahan, A., Ibrahim, H., Soliman, M., Ebrahim, S., 2019. Polyaniline/akaganéite superparamagnetic nanocomposite for cadmium uptake from polluted water. Desalin. Water Treat. 171, 205–215.
Sips, R.J., 1948. On the structure of a catalyst surface. J. Chem. Phys. 16, 490–495.
To, M., Hadi, P., Hui, C., Lin, C., McKay, G., 2017. Mechanistic study of atenolol, acebutolol and carbamazepine adsorption on waste biomass derived activated carbon. J. Molecular Liquids. 241, 386–398.
Tome, S., Dzoujo, H., Shikuku, V., Otieno, S., 2021. Synthesis, characterization and application of acid and alkaline activated volcanic ash-based geopolymers for adsorptive remotion of cationic and anionic dyes from water. Ceram. Int. 47 (15), 20965–20973. https://doi.org/10.1016/j.ceramint.2021.04.097.
Treybal, R.E., 1981. Mass-transfer Operations, 3rd ed. McGraw-Hill.
Volesky, B., 2007. Biosorption and me. Water Res. 41, 4017–4029.
Wu, L., Zhang, S., Wang, J., Ding, X., 2020. Phosphorus retention using iron (II/III) modified biochar in saline-alkaline soils: Adsorption, column and field tests. Environ. Pollut. 261, 114223 https://doi.org/10.1016/j.envpol.2020.114223.
Yang, Q., Wang, X., Luo, W., Sun, J., Xu, Q., Chen, F., Zhao, J., Wang, S., Yao, F., Wang, D., Li, X., Zeng, G., 2017. Effectiveness and mechanisms of phosphate adsorption on iron-modified biochars derived from waste activated sludge. Biores. Technol. 247, 537–544. https://doi.org/10.1016/j.biortech.2017.09.136.
Zhang, M., Gao, B., Varnoosfaderani, S., Hebard, A., Yao, Y., Inyang, M., 2013. Preparation and characterization of a novel magnetic biochar for arsenic removal. Bioresou. Technol. 130, 457–462. https://doi.org/10.1016/j.biortech.2012.11.132.
Zhang, Y., Geißen, S.U., Gal, C., 2008. Carbamazepine and diclofenac: Removal in wastewater treatment plants and occurrence in water bodies. Chemosphere. 73 (8), 1151–1161.
Zheng, L., Yang, Y., Meng, P., Peng, D., 2019. Absorption of cadmium (II) via sulfur-chelating based cellulose: Characterization, isotherm models and their error analysis. Carbohydr. Polymers. 209, 38–50.